Int. J. Electrochem. Sci., 8 **(2013)** 3676 - 3686

International Journal of
ELECTROCHEMICAL
SCIENCE
www.electrochemsci.org

Electrochemical Properties of Spherical Hollow SnO_2-TiO_2-C Composite Powders Prepared by Spray Pyrolysis

*Min Ho Kim, Yun Chan Kang**

Department of Chemical Engineering, Konkuk University, 1 Hwayang-dong, Gwangjin-gu, Seoul 143-701, Korea
*E-mail: yckang@konkuk.ac.kr

Received: 9 January 2013 / *Accepted:* 3 February 2013 / *Published:* 1 March 2013

Hollow spherical SnO_2-TiO_2-C composite powders with uniform compositions are prepared by spray pyrolysis from precursor solutions containing Sn and Ti compounds along with citric acid and ethylene glycol. The prepared composite powders are subsequently heat-treated at various temperatures. Samples treated at 400 °C show the presence of amorphous structures and fine crystallites with sizes ranging to a few nanometers. Crystalline peaks corresponding to rutile-like crystal structures are observed in the XRD patterns of the composite powders treated at 600 °C. The peaks in the XRD patterns of the SnO_2 phase with the rutile structure marginally shift to higher angles because of the formation of the SnO_2-TiO_2 solid solution. Crystals with sizes below 10 nm present in composite powders treated at 600 °C are coated with a layer of amorphous carbon. Phase separation of Sn and Ti components dose not occur during the crystallization of the composite powders by heat-treatment. The cycle performances of the SnO_2-TiO_2-C composite powders are better than that of pure SnO_2 powders at a constant charge and discharge rate of 700 mA g^{-1} in the voltage range 0.01–3.0 V. The discharge capacities after 50 cycles for the composite powders treated at 600 °C are 394, 396, 327, and 244 mAh g^{-1} at discharge rates of 300, 1400, 2100, and 3500 mA g^{-1}, respectively.

Keywords: tin oxide; composite powders; anode material; spray pyrolysis; lithium battery

1. INTRODUCTION

The use of SnO_2-based materials as anode materials in Li-ion batteries has been widely studied owing to their high theoretical capacity, low cost, and safety [1-3]. However, the large volume changes (up to 300%) occurring during Li^+ insertion or exclusion causes acute mechanical damage to the electrode, resulting in poor cycle performances [4-6].

Many studies have aimed at improving the fatal capacity fading of SnO_2-based electrodes [7-10]. One effective approach is the development of nanostructured electrode materials [11-15]. Nanostructured electrode materials facilitate rapid Li^+ insertion or extraction due to the short diffusion

distances in small grains and accommodate the associated volume change [16]. In addition, empty spaces in nanostructured powders can also tolerate the occurrence of large volume changes during cycling [10,17-19]. Therefore, hollow and/or porous nanostructured SnO_2-based electrodes have been reported to exhibit improved cycle performances and high rate capabilities [18,20-23]. Another commonly used approach is to use active/active and active/inactive nanocomposite electrodes [24]. The inactive or active component that do not undergo volume change during cycling buffer the large volume change that occurs during Li^+ insertion or extraction [25-27].

TiO_2 has been reported show promise as an anode material that can be used in Li-ion batteries owing to its enhanced capacity retention, superior rate performance, and lower self-discharge rate [1,28-30]. Although theoretical capacities as high as 335 mA h g^{-1} have been calculated for the insertion of one Li^+ per TiO_2 molecule, the poor ionic and electronic conductivities limit the capacity to 168 mAh g^{-1} [31-32]. Recently, many approaches including reducing the particle size to decrease the Li^+ diffusion length and preparing TiO_2 composite structures to improve charge transfer have been devised to improve the capacity [33-36]. Electrochemically active TiO_2-based materials that show negligible volume change during Li^+ insertion or extraction could be effectively used as buffers in combination with SnO_2-based materials to form composite powders. These powders may be expected to exhibit high capacities and enhanced cycle performances [37-39]. Park et al. showed that SnO_2 encapsulated hollow TiO_2 nanofibers exhibit improved electrochemical performances when compared with unencapsulated hollow TiO_2 nanofibers and show a high initial charge capacity of ~517 mAh g^{-1} at 0.2 C [5]. Lin et al. prepared TiO_2-supported SnO_2 nanocomposites by co-precipitation. The anode, composed of amorphous TiO_2-cassiterite SnO_2, retained a reversible capacity of 320 mAh g^{-1} depending on the weight ratio of SnO_2 to TiO_2 at 0.2 C after 100 cycles [6].

Spray pyrolysis is reported to be advantageous for the large-scale and continuous production of multicomponent oxide powders [40]. Spray pyrolysis, which involves reactions at the microscale within the micron-sized droplets, also permits the fine control of the morphologies of the product nanocomposite powders [41-47]. In this study, hollow spherical SnO_2-TiO_2-C nanocomposite powders with fine grains of sizes ranging to a few nanometers were prepared by spray pyrolysis. The effects of the presence of various crystal structures and morphologies of the particles in the powders on the electrochemical properties of the composite were investigated.

2. EXPERIMENTAL

SnO_2 (50 wt%)-TiO_2 (50 wt%) composite powders were prepared by spray pyrolysis. The equipment used for the preparation consisted of six ultrasonic spray generators operated at 1.7 MHz, a tubular quartz reactor (length = 1000 mm; inner diameter = 50 mm), and a bag filter. The precursor materials were tin sulfate ($SnSO_4$, Junsei Chemicals) and titanium tetraisopropoxide (TTIP, Junsei Chemicals). A small amount of nitric acid was used to peptize the hydrolyzed TTIP to form a clear solution. The overall concentration of the Sn and Ti components in the precursor solution was 0.1 M. Citric acid monohydrate (Samchun Chemicals) and ethylene glycol (Samchun Chemicals) were used as chelating agents and as carbon sources to improve the hollowness of the precursor particles. The

concentrations of citric acid and ethylene glycol were 0.2 M and 0.1M, respectively. The spray pyrolysis was carried out at a fixed temperature of 900 °C. The flow rate of air, which was used as the carrier gas in the reaction, was fixed at 40 L min^{-1}. The precursor powders prepared by spray pyrolysis were heat-treated at temperatures in the range 200–800 °C for 3 h under air.

The crystal structures of the as-prepared and heat-treated powders were investigated using X-ray diffractometry (XRD, X'Pert PRO MRD) using Cu Kα radiation (wavelength $\lambda = 1.5418 \times 10^{-10}$ m, θ = 20–80˚) at the Korea Basic Science Institute (Daegu). The morphological characteristics of the powders were investigated using scanning electron microscopy (SEM, JEOL JSM-6060) and high-resolution transmission electron microscopy (HRTEM, JEOL-2100F). The surface areas of the powders were measured by the Brunauer–Emmett–Teller (BET) method with N_2(g) as the adsorbate. The electrochemical characteristics of the SnO_2-TiO_2 composite powders were examined by fabricating 2032 coin cells. The working electrodes were prepared by coating a slurry containing a mixture of the active material (80 wt%), sodium carboxymethyl cellulose (CMC) binder (10 wt%), and conductive carbon (Super P) (10 wt%) on copper foil substrates. Then, the electrode films were dried at 100 °C in an oven, overnight. The loading of the active material within the film was about 3 mg cm^{-2}. Lithium foil served as the counter electrode and a polypropylene film was used as the separator. $LiPF_6$ (1 M) in a mixture of ethylene carbonate (EC) and dimethyl carbonate (DMC) in a 1:1 volume ratio with 2 wt% vinylene carbonate (VC) was used as the electrolyte (Techno Semichem. Co.). The entire cell was assembled in a glove box under an atmosphere of argon. The charge/discharge characteristics of the samples were measured by cycling in the potential range 0.01–3.0 V at various current densities. Cyclic voltammetry measurements were carried out at a scan rate of 0.1 mV s^{-1}.

3. RESULTS AND DISCUSSION

The morphologies and crystal structures of the SnO_2-TiO_2 composite powders before and after heat-treatment at temperatures in the range 200–800 °C are shown in Figs. 1 and 2. The precursor powders (prior to the heat-treatment) exhibited hollow structures with sizes in the order of microns and were black in color. Decomposition and carbonization of the polymer formed by the esterification of citric acid with ethylene glycol produced the black carbon in the composite powders. Abrupt evolution of gases due to the decomposition of the organic polymer and metal salts formed the hollow-structured composite powders. Consequently, every single hollow SnO_2-TiO_2-C composite powder particle was formed from a single droplet. The morphologies of the precursor powders were retained after the heat-treatment at 800 °C for 3 h under an atmosphere of air. The precursor and composite powders treated at temperatures below 400 °C showed amorphous structures. Crystalline peaks were observed in the XRD patterns of composite powders treated at temperatures above 600 °C, as shown in Fig. 2. These XRD patterns showed the presence of a single phase with rutile-type crystal structure and trace diffraction peaks due to the presence of other phases were absent. In the XRD patterns, slight shifts of the peaks corresponding to the rutile (cassiterite) phase of SnO_2 to higher angles occurred due to the formation of SnO_2-TiO_2 solid solution caused by the use of high treatment temperatures of 600 and 800 °C.

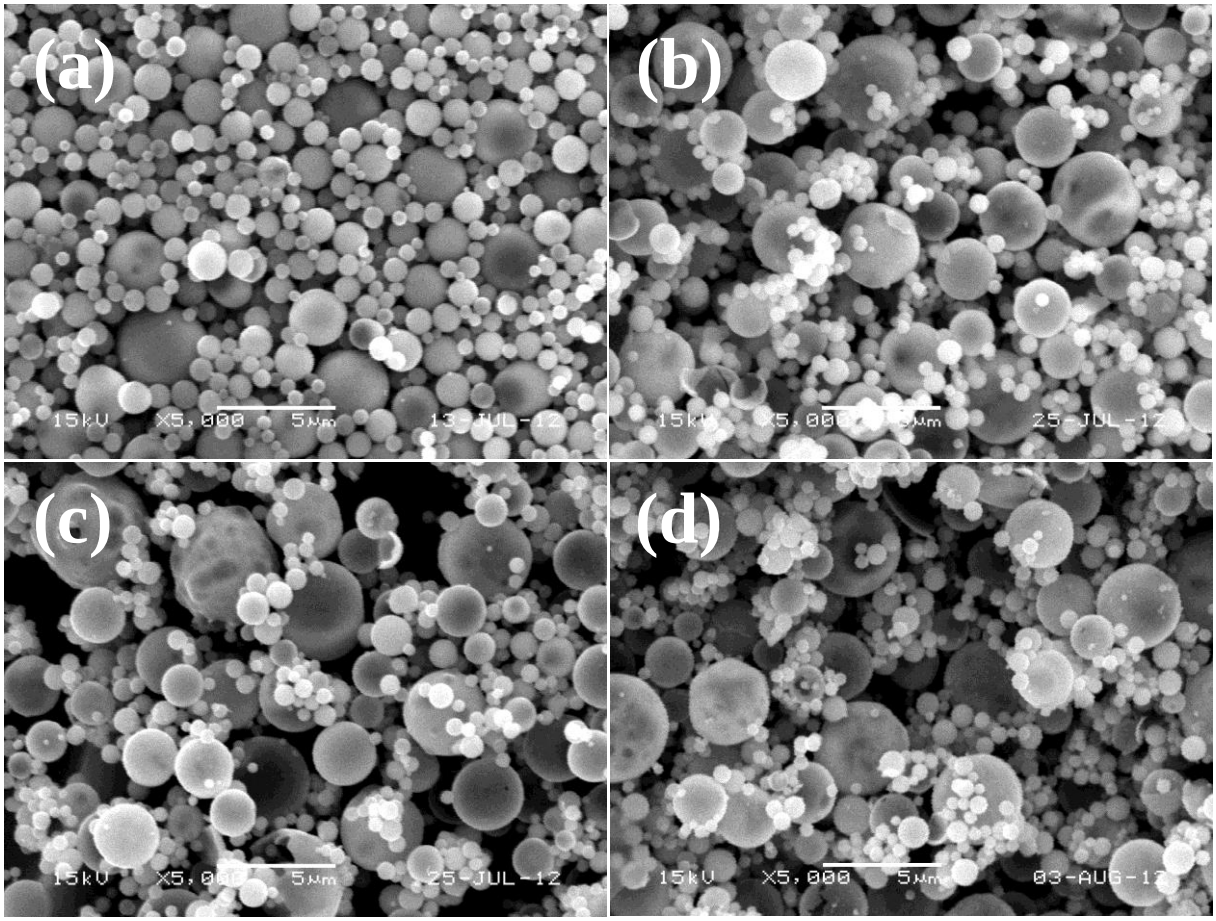

Figure 1. SEM images of the SnO_2-TiO_2-C composite powders prepared by spray pyrolysis (a) before post-synthesis heat-treatment and after treatment at (b) 400 °C, (c) 600 °C, and (d) 800 °C.

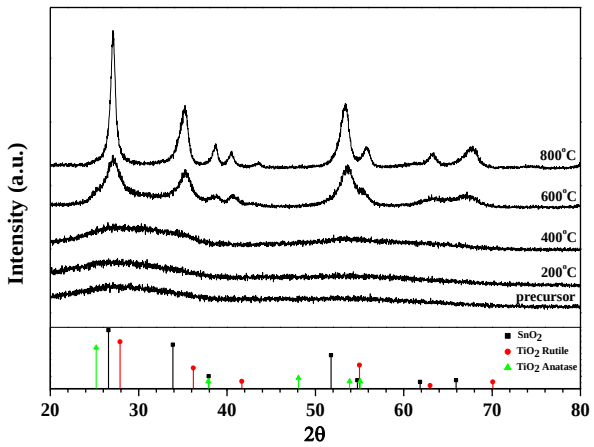

Figure 2. XRD patterns of the SnO_2-TiO_2-C composite powders prepared by spray pyrolysis before and after heat-treatment at various temperatures.

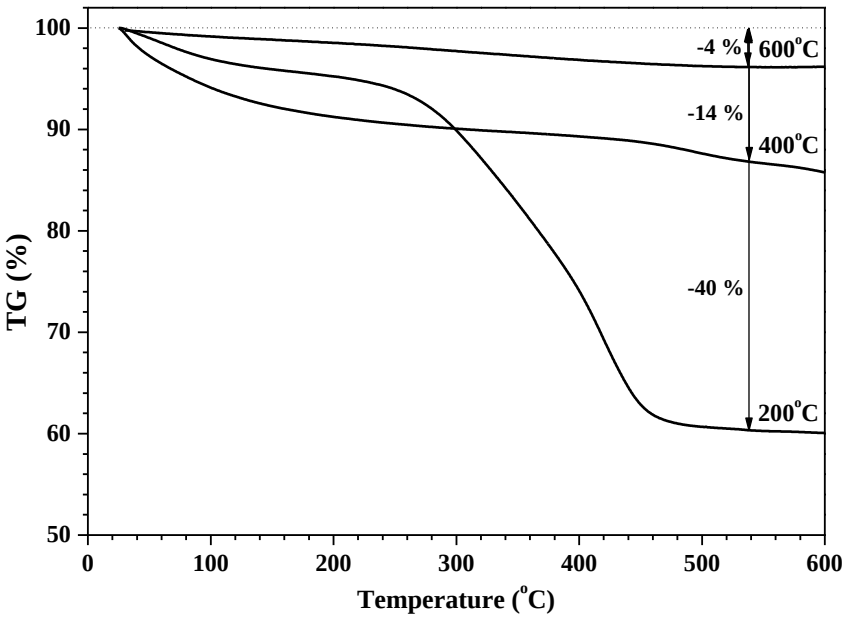

(a) TGA

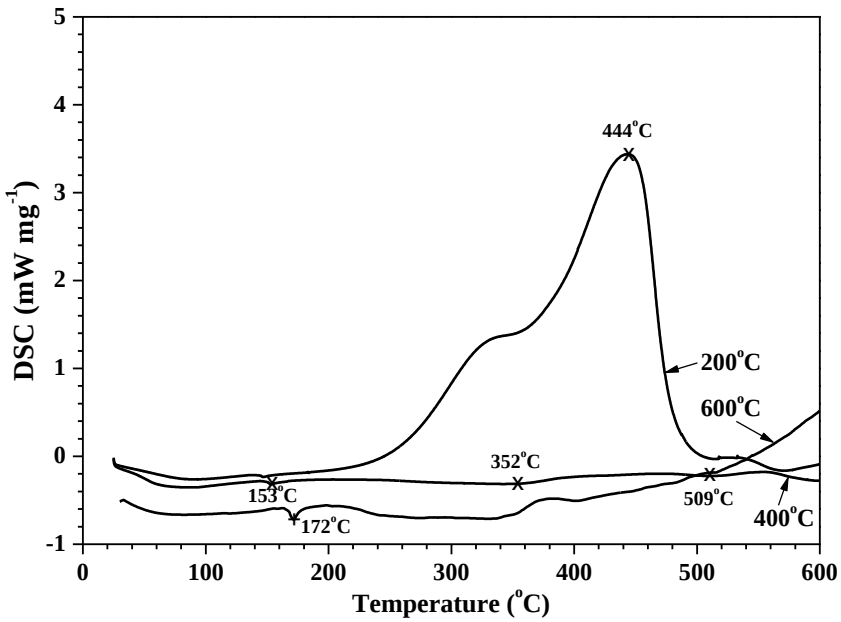

(b) DSC

Figure 3. TG/DSC curves of the SnO_2-TiO_2-C composite powders treated at various temperatures after preparation by spray pyrolysis.

Fig. 3 shows the TG/DSC curves of the SnO_2-TiO_2-C composite powders treated at 200, 400, and 600 °C. In the TG curves, two major weight losses were observed between room temperature and 600 °C. The first conspicuous weight loss region in the temperature range 40–200 °C resulted from the loss of adsorbed water. The second region of weight loss in the temperature range 250–600 °C resulted from the decomposition of the carbon component in the composite powders. When the powders were heated at temperatures ranging up to 600 °C, mass losses of 40, 14, and 4 wt% were observed in the TG curves of the composite powders treated at 200, 400, and 600 °C. The results of the DSC analysis

of the composite powders treated at 200 °C showed two exothermic peaks at 353 °C and 444 °C due to the decomposition of the carbon components.

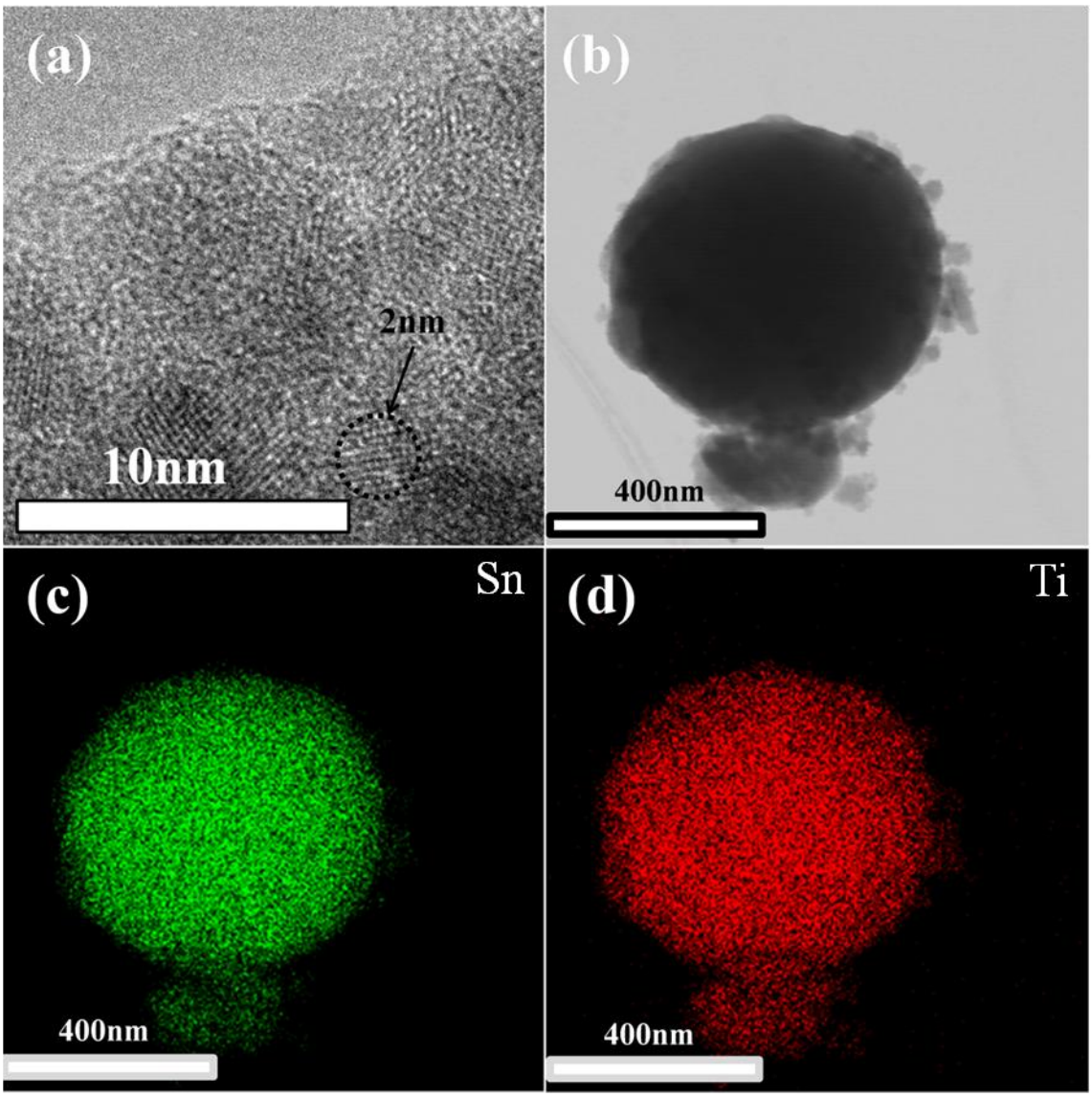

Figure 4. TEM images and elemental distribution dot maps of SnO_2-TiO_2-C composite powders treated at 400 °C.

The SnO_2-TiO_2-C composite powders treated at 400 and 600 °C were crushed using an agate mortar to prepare the TEM samples. Figs. 4 and 5 show the TEM images of the samples and dot maps of elemental distribution in the composite powder samples. The HRTEM image of the composite powders treated at 400 °C shown in Fig. 4 (a) exhibited the presence of fine crystallites that were a few nanometers in size dispersed in the amorphous matrix. The SnO_2-TiO_2-C composite powders treated at 400 °C was amorphous and contained high amounts of the carbon component, as observed from the XRD pattern and TG curve shown in Fig. 2 and Fig. 3. Therefore, it can be inferred that in these

samples, only a small amount of the Sn and Ti components formed the nanometer-sized crystals. The amorphous phase was a mixture of Sn, Ti, and carbon components.

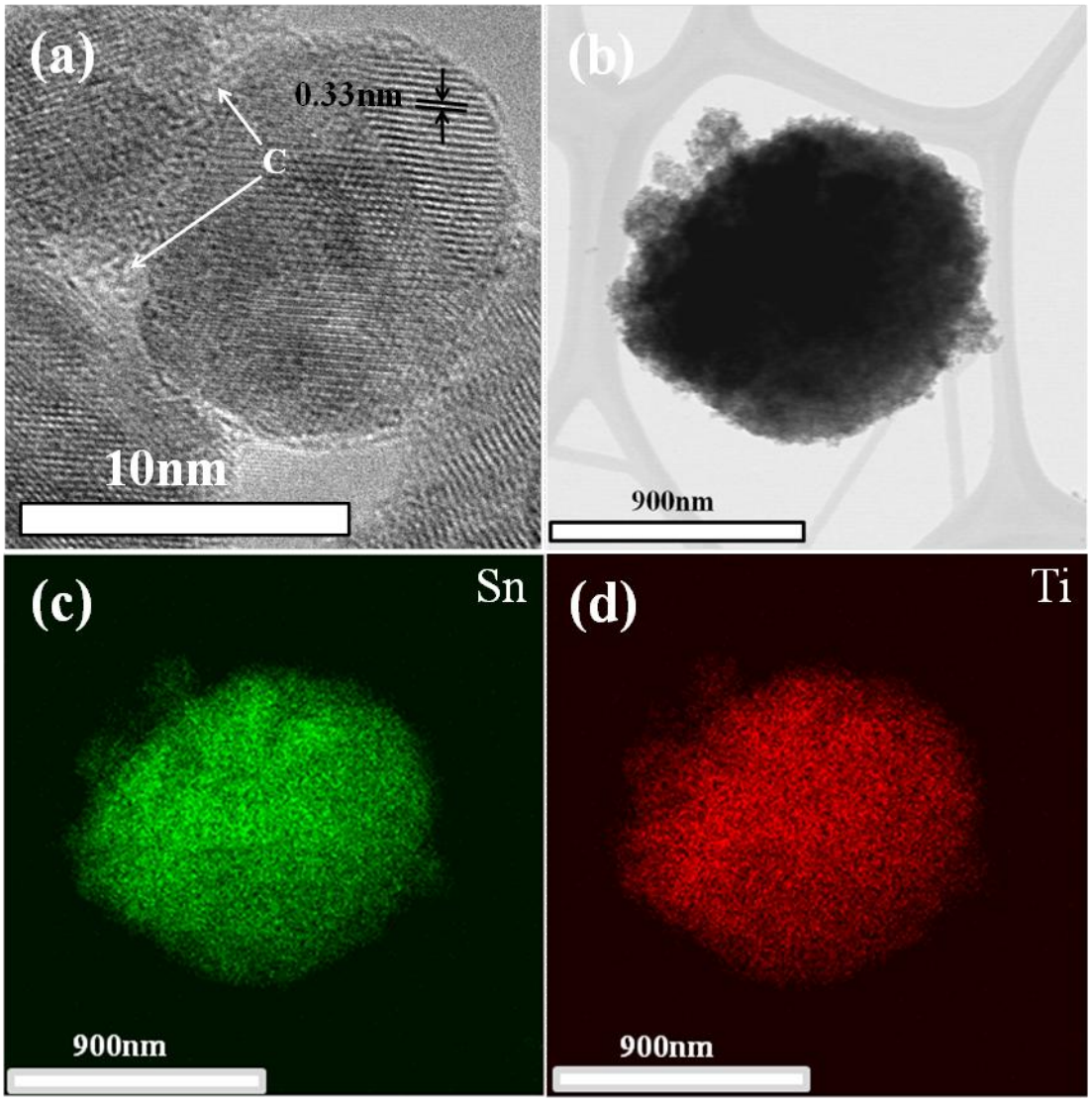

Figure 5. TEM images and elemental distribution dot maps of SnO_2-TiO_2-C composite powders treated at 600 °C.

Crystal growth in the composite powders occurred when the samples were treated at 600 °C. The crystals with sizes ranging below 10 nm were coated with an amorphous carbon layer, as shown by the HRTEM image in Fig. 5 (a). The results of dot mapping of the elemental distribution in the composite powders treated at 400 and 600 °C shown in Fig. 4 and Fig. 5 revealed the uniform distribution of Sn and Ti components over the entirety of the samples. Phase separation of Sn and Ti components did not occur during crystallization by heat-treatment because of the formation of a solid solution.

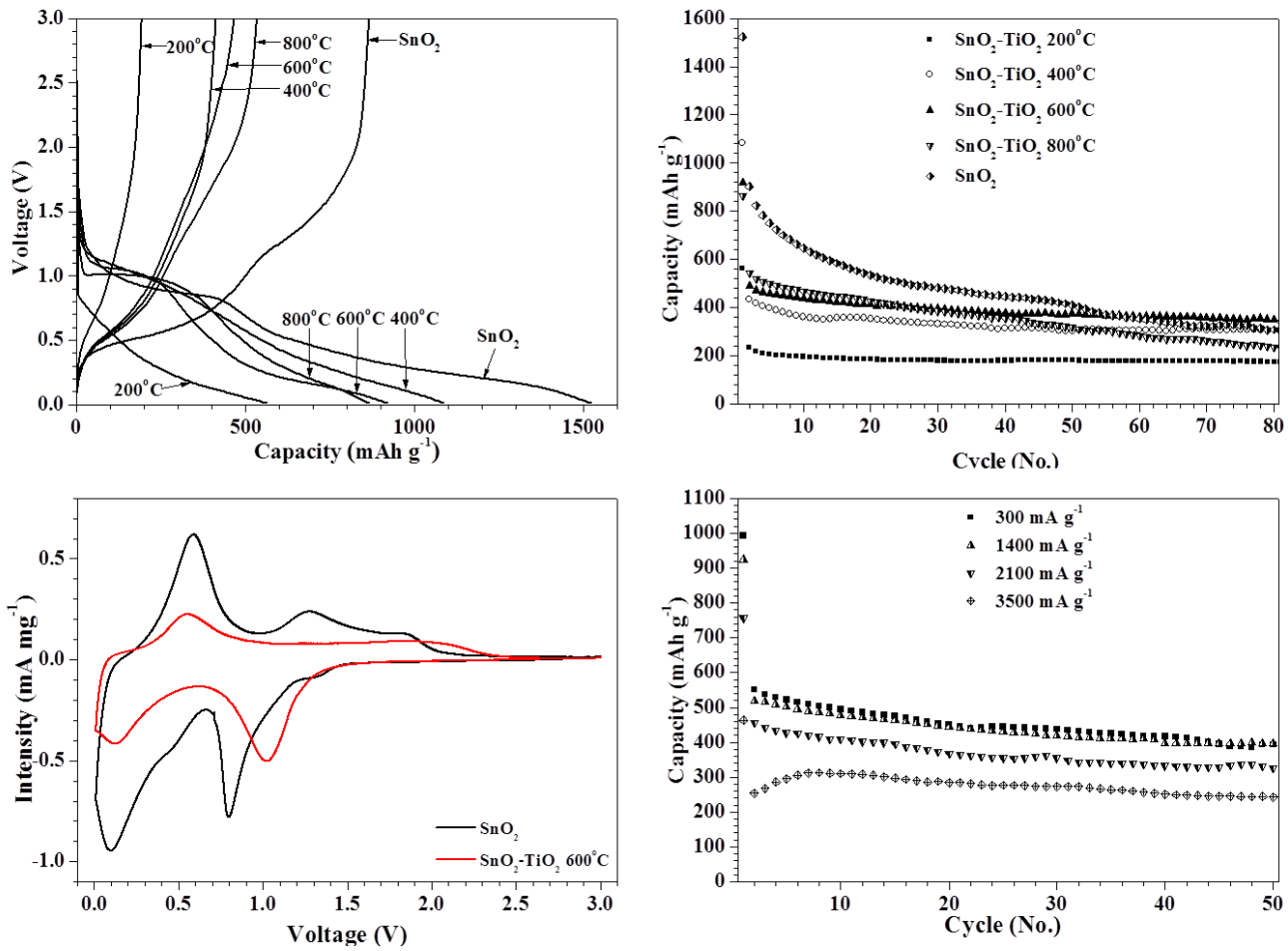

Figure 6. (a) Initial charge and discharge curves and (b) cycling performances of pure SnO_2 and SnO_2-TiO_2-C composite powders at a constant charge and discharge rate of 700 mA g^{-1}. (c) Cyclic voltammograms of pure SnO_2 and SnO_2-TiO_2 composite powders at a scan rate of 0.1 mV s^{-1}. (d) Cycling performances at various discharge rates of the SnO_2-TiO_2 composite powders treated at 600 °C after synthesis by spray pyrolysis.

The electrochemical properties of the SnO_2-TiO_2-C composite powders treated at temperatures in the range 200–800 °C were compared with that of the pure SnO_2 powders. The pure SnO_2 powder samples prepared by spray pyrolysis were spherical in shape and exhibited porous structures after treatment at 600 °C. Fig. 6 (a) and (b) show the initial charge and discharge curves and cycle performances of the pure SnO_2 and SnO_2-TiO_2-C composite powders at a constant charge and discharge rate of 700 mA g^{-1} in the range 0.01–3.0 V. The shapes of the initial charge and discharge curves of the composite powders treated at temperatures above 400 °C and that of the pure SnO_2 powders were similar. In these curves, distinct potential plateaus at ~1.0 V, attributed to the reduction of Sn(IV) to Sn(0), were observed [1,2]. The plateaus at ~1.5 V, attributed to the reduction of Ti(IV) to Ti(III), were absent in the initial discharge curves of the solid solution composite powders. In addition, the plateau at ~1.0 V was also absent in the initial discharge curve of the amorphous SnO_2-TiO_2 composite powders obtained by heat-treatment at 200 °C. The initial charge and discharge capacities of the pure SnO_2 powders were 866 and 1523 mAh g^{-1} and the Coulombic efficiency was 57%. In

contrast, the initial discharge capacities of the SnO_2-TiO_2-C composite powders treated at 200, 400, 600, and 800 °C were 562, 1085, 919, and 865 mAh g^{-1}, respectively, and the Coulombic efficiencies of the first cycles were 34, 38, 51, and 62%, respectively. The BET surface areas of the composite powders treated at 400, 600, and 800 °C were 95, 29, and 12 m^2 g^{-1}, respectively. The composite powders treated at temperatures below 600 °C showed low initial Coulombic efficiencies because a solid electrolyte interphase (SEI) layer was formed on the external surface of the composite powders that exhibit high surface areas. The discharge capacity of the pure SnO_2 powder samples decreased from 1523 to 308 mAh g^{-1} after 80 cycles. However, the discharge capacities of the SnO_2-TiO_2-C composite powders treated at 200, 400, 600, and 800 °C after 80 cycles were 175, 305, 350, and 234 mA h g^{-1}, respectively. Hence, the SnO_2-TiO_2 composite powders showed better cycle performances than that of the pure SnO_2 powders. Fig. 6 (c) shows the cyclic voltammograms (CVs) of the pure SnO_2 and SnO_2-TiO_2-C composite powders during the first cycle measured at a scan rate of 0.1 mV s^{-1} in the voltage range 0.01–3.0 V. The presence of reduction peaks at around 0.8 and 1 V in the CV profiles of the pure SnO_2 and SnO_2-TiO_2 composite powders in the initial cycles clearly indicated that an irreversible reaction had occurred during the initial discharge. The reduction peak shifted to higher voltages due to the formation of SnO_2-TiO_2 solid solutions. These reduction peaks disappeared in the CV profiles during the second cycles and only peaks at low potentials (at <0.5 V) corresponding to the formation of Li-Sn alloy were observed [48,49]. Fig. 6 (d) shows the cycle performances of the SnO_2-TiO_2-C composite powders treated at 600 °C at constant discharge rates ranging between 300 and 3500 mA g^{-1} in the voltage range 0.01–3.0 V. The charge rate was fixed at 300 mA g^{-1}. The initial discharge capacities of the composite powders were 992, 924, 756, and 464 mAh g^{-1} at discharge rates of 300, 1400, 2100, and 3500 mA g^{-1}, respectively. The discharge capacities monotonically decreased with increasing cycle numbers, except at a high discharge rate of 3500 mA g^{-1}. The discharge capacity increased from 254 to 313 mAh g^{-1} for the first seven cycles at a discharge rate of 3500 mA g^{-1}. The discharge capacities were 394, 396, 327 and 244 mAh g^{-1} after 50 cycles at discharge rates of 300, 1400, 2100, and 3500 mA g^{-1}, respectively. The discharge capacity retentions measured after the initial cycle at discharge rates of 300, 1400, and 2100 mA g^{-1} were 72%, 76%, and 72 %, respectively, after 50 cycles. Therefore, the SnO_2-TiO_2-C composite powders prepared by spray pyrolysis exhibited high discharge capacities, good cycle retention, and high rate performances.

4. CONCLUSIONS

Spherical hollow SnO_2-TiO_2-C nanocomposite powders with amorphous structures were prepared by spray pyrolysis. The composite powders treated at a low temperature of 200 °C after synthesis by spray pyrolysis showed poor electrochemical performances. The optimum heat-treatment temperature required for obtaining SnO_2-TiO_2-C nanocomposite powders with high discharge capacities and high rate performances was 600 °C. The composite powders treated at 600 ^oC consisted of fine crystallites and showed uniform distribution of Sn and Ti components over the entire sample. However, pure SnO_2 powders prepared by spray pyrolysis showed comparatively poor cycle properties at a constant charge and discharge rate of 700 mA g^{-1} in the voltage range 0.01–3.0 V. In contrast, the

SnO_2-TiO_2-C composite powders exhibited high capacities and good cycle properties even at a high discharge rates ranging to 2100 mA g^{-1}.

ACKNOWLEDGEMENT
This work was supported by the National Research Foundation of Korea (NRF) grant funded by the Korea government (MEST) (No. 2012R1A2A2A02046367). This research was supported by Basic Science Research Program through the National Research Foundation of Korea (NRF) funded by the Ministry of Education, Science and Technology (2012R1A1B3002382). This work was supported by Seoul R&BD Program (WR090671).

References

1. D. Deng, M.G. Kim, J.Y. Lee, J. Cho, *Energy Environ. Sci.*, 2 (2009) 818.
2. J.S. Chen, L.A. Archer, X.W. Lou, *J. Mater. Chem.*, 21 (2011) 9912.
3. J.S. Chen, X.W. Lou, *Mater. Today*, 15 (2012) 246.
4. J.S. Chen, D.Y. Luan, C.M. Li, F.Y.C. Boey, S.Z. Qiao, X.W. Lou, *Chem. Commun.*, 46 (2010) 8252.
5. H.J. Park, T.S. Song, H.K. Han, A. Devadoss, J.H. Yuh, C.H. Choi, U. Paik, *Electrochem. Commun.*, 22 (2012) 84.
6. Y.M. Lin, R.K. Nagarale, K.C. Klavetter, A. Heller, C.B. Mullins, *J. Mater. Chem.*, 22 (2012) 11134.
7. J. Fan, T. Wang, C. Yu, B. Tu, Z. Jiang, D. Zhao, *Adv. Mater.*, 16 (2004) 1432.
8. G.D. Du, C. Zhong, P. Zhang, Z.P. Guo, Z.X. Chen, H.K. Liu, *Electrochim. Acta*, 55 (2010) 2582.
9. Y. Wang, F. Su, J.Y. Lee, X.S. Zhao, *Chem. Mater.*, 18 (2006) 1347.
10. K.T. Lee, Y.S. Jung, S.M. Oh, *J. Am. Chem. Soc.*, 125 (2003) 5652.
11. Z.W. Zhao, Z.P. Guo, D. Wexler, Z.F. Ma, X. Wu, H.K. Liu, *Electrochem. Commun.*, 9 (2007) 697.
12. Y. Liang, J. Fan, X. Xia, Z. Jia, *Mater. Lett.*, 61 (2007) 4370.
13. M.S. Park, G.X. Wang, Y.M. Kang, D. Wexler, S.X. Dou, H.K. Liu, *Angew. Chem. Int. Ed.*, 46 (2007) 750.
14. Y.D. Ko, J.G. Kang, J.G. Park, S.J. Lee, D.W. Kim, *Nanotechnology*, 20 (2009) 455701.
15. Y. Wang, J.Y. Lee, H.C. Zeng, *Chem. Mater.*, 17 (2005) 3899.
16. A.S. Arico, P. Bruce, B. Scrosati, J.M. Tarascon, W. Van Schalkwijk, *Nat. Mater.*, 4 (2005) 366.
17. X.W. Lou, C.M. Li, L.A. Archer, *Adv. Mater.*, 21 (2009) 2536.
18. S.J. Han, B.C. Jang, T.A. Kim, S.M. Oh, T.H. Hyeon, *Adv. Funct. Mater.*, 15 (2005) 1845.
19. X.W. Lou, L.A. Archer, Z. Yang, *Adv. Mater.*, 20 (2008) 3987.
20. D. Deng, J.Y. Lee, *Chem. Mater.*, 20 (2008) 1841.
21. X.W. Lou, D. Deng, J.Y. Lee, L.A. Archer, *Chem. Mater.*, 20 (2008) 6562.
22. Y. Wang, H.C. Zeng, J.Y. Lee, *Adv. Mater.*, 18 (2006) 645.
23. L. Yuan, Z.P. Guo, K. Konstantinov, J.Z. Wang, H.K. Liu, *Electrochim. Acta*, 51 (2006) 3680.
24. M. Winter, J.O. Besenhard, *Electrochim. Acta*, 45 (1999) 31.
25. D. Zhang, C. Yang, J. Dai, J. Wen, L. Wang, C. Chen, *Trans. Nonferrous Met. Soc. China*, 19 (2009) 1489.
26. S.M. Hasanaly, M.A. Bustam, *J. Eng. Sci.*, 7 (2011) 15.
27. B. Scrosati, J. Garche, *J. Power Sources*, 195 (2010) 2419.
28. J.Y. Kim, J.P. Cho, *J. Electrochem. Soc.*, 154 (2007) A542.
29. A.R. Armstrong, G. Armstrong, J. Canales, P.G. Bruce, *Angew. Chem. Int. Ed.*, 43 (2004) 2286.
30. J.S. Chen, Y.L. Tan, C.M. Li, Y.L. Cheah, D. Luan, S. Madhavi, F.Y.C. Boey, L.A. Archer, X.W. Lou, *J. Am. Chem. Soc.*, 132 (2010) 6124.

31. T. Fröschl, U. Hörmann, P. Kubiak, G. Kučerová, M. Pfanzelt, C.K. Weiss, R.J. Behm, N. Hüsing, U. Kaiser, K. Landfester, M. Wohlfahrt-Mehrens, *Chem. Soc. Rev.*, 41 (2012) 5313.
32. M. Inaba, Y. Oba, F. Niina, Y. Murota, Y. Ogino, A. Tasaka, K. Hirota, *J. Power Sources*, 189 (2009) 580.
33. C. Jiang, M. Wei, Z. Qi, T. Kudo, I. Honma, H. Zhou, *J. Power Sources*, 166 (2007) 239.
34. V. Subramanian, A. Karki, K.I. Gnanasekar, F.P. Eddy, B. Rambabu, *J. Power Sources*, 159 (2006) 186.
35. L.J. Fu, H. Liu, H.P. Zhang, C. Li, T. Zhang, Y.P. Wu, H.Q. Wu, J. Power Sources, 159 (2006) 219.
36. S.H. Yoon, B.H. Ka, C.W. Lee, M.S. Park, S.M. Oh, *Electrochem. Solid-State Lett.*, 12 (2009) A28.
37. J.F. Lei, W.S. Li, X.P. Li, E.J. Cairns, *J. Mater. Chem.*, 22 (2012) 22022.
38. S.J. Bao, Q.L. Bao, C.M. Li, Z.L. Dong, *Electrochem. Commun.*, 9 (2007) 1233.
39. J. Yi, X. Li, S. Hu, W. Li, R. Zeng, Z. Fu, L. Chen, *Rare Met.*, 30 (2011) 589.
40. D.S. Jung, S.B. Park, Y.C. Kang, *Korean J. Chem. Eng*., 27 (2010) 1621.
41. C.M. Sim, Y.J. Hong, M.H. Kim, Y.S. Jang, B.K. Park, Y.C. Kang, *Int. J. Electrochem. Sci.*, 7 (2012) 12110.
42. Y.H. Choa, J.K. Yang, B.H. Kim, Y.K. Jeong, J.S Lee, T. Nakayama, T. Sekino, K. Niihara, *J. Magn. Magn. Mater.*, 266 (2003) 12.
43. Y.S. Jang, J.H. Kim, J.K. Lee, B.K. Park, Y.C. Kang, *Int. J. Electrochem. Sci.*, 7 (2012) 12370.
44. K. Matsuda, I. Taniguchi, *J. Power Sources*, 132 (2004) 156.
45. Y.N. Ko, J.H. Kim, J.K. Lee, Y.C. Kang, J.H. Lee, *Electrochim. Acta*, 69 (2012) 345.
46. Y.J. Hong, S.H. Choi, C.M. Sim, J.K. Lee, Y.C. Kang, *Mater. Res. Bull.*, 47 (2012) 4359.
47. S.H. Choi, J.H. Kim, Y.N. Ko, Y.J. Hong, Y.C. Kang, *J. Power Sources*, 210 (2012) 110.
48. X.W. Lou, Y. Wang, C. Yuan, J.Y. Lee, L.A. Archer, *Adv. Mater.*, 18 (2006) 2325.
49. M. Mohamedi, S.J. Lee, D. Takahashi, M. Nishizawa, T. Itoh, I. Uchida, *Electrochim. Acta*, 46 (2001) 1161.

© 2013 by ESG (www.electrochemsci.org)